



HAL
open science

Coordination Polymers as Template for Mesoporous Silica Films: A Novel Composite Material Fe(Htrz)₃@SiO₂ with Remarkable Electrochemical Properties

Samuel Ahoulou, Neus Vilà, Sébastien Pillet, Dominik Schaniel, Alain Walcarius

► To cite this version:

Samuel Ahoulou, Neus Vilà, Sébastien Pillet, Dominik Schaniel, Alain Walcarius. Coordination Polymers as Template for Mesoporous Silica Films: A Novel Composite Material Fe(Htrz)₃@SiO₂ with Remarkable Electrochemical Properties. *Chemistry of Materials*, 2019, 31 (15), pp.5796-5807. 10.1021/acs.chemmater.9b01879 . hal-02324674

HAL Id: hal-02324674

<https://hal.science/hal-02324674>

Submitted on 26 Nov 2020

HAL is a multi-disciplinary open access archive for the deposit and dissemination of scientific research documents, whether they are published or not. The documents may come from teaching and research institutions in France or abroad, or from public or private research centers.

L'archive ouverte pluridisciplinaire **HAL**, est destinée au dépôt et à la diffusion de documents scientifiques de niveau recherche, publiés ou non, émanant des établissements d'enseignement et de recherche français ou étrangers, des laboratoires publics ou privés.

Coordination polymers as template for mesoporous silica films: a novel composite material $\text{Fe}(\text{Htrz})_3@ \text{SiO}_2$ with remarkable electrochemical properties

Samuel Ahoulou,^{a,b} Neus Vilà,^a Sébastien Pillet,^b Dominik Schaniel^b and Alain Walcarius^{a*}

^a *Laboratoire de Chimie Physique et Microbiologie pour les Matériaux et l'Environnement (LCPME), UMR 7564 CNRS – Université de Lorraine, 405 rue de Vandoeuvre, 54600 Villers-lès-Nancy (France)*

^b *Université de Lorraine, CNRS, CRM2 UMR7036, 54000 Nancy, France*

** Corresponding author e-mail: alain.walcarius@univ-lorraine.fr*

Abstract

While attempting to confine $\text{Fe}(\text{Htrz})_3$ ($\text{Htrz} = 1,2,4, \text{-}1H\text{-triazole}$) into a mesoporous silica matrix during its formation by electrochemically assisted self-assembly (EASA), we have discovered that such spin crossover complex is likely to act as the template (in place of the surfactant species) to form in one step a composite mesoporous material ($\text{Fe}(\text{Htrz})_3@ \text{SiO}_2$). The EASA method usually leads to the vertical growth of mesoporous silica thin films owing to the electro-induced condensation of silica precursors (i.e., tetraethoxysilane, TEOS) around tubular micelles (i.e., made of cetyltrimethylammonium bromide, CTAB) oriented orthogonally to the underlying support. In the presence of $\text{Fe}(\text{Htrz})_3$ in the starting sol (in addition to TEOS and CTAB), two distinct situations can be reached. At low $\text{Fe}(\text{Htrz})_3$ concentration (≤ 3 mM), the vertically aligned mesostructure is formed and $\text{Fe}(\text{Htrz})_3$ complexes are incorporated along with the surfactant phase, but most of them are released upon surfactant removal. At high $\text{Fe}(\text{Htrz})_3$ concentration (typically 5 mM), a wormlike mesoporous film is obtained in which $\text{Fe}(\text{Htrz})_3$ species act as a real template for the formation of a mesoporous $\text{Fe}(\text{Htrz})_3@ \text{SiO}_2$ film. Interestingly, the iron-triazole

complex is strongly entrapped in the silica matrix as it cannot be removed by solvent extraction (contrary to CTAB), as evidenced from X-ray photoelectron spectroscopy (XPS). Even more attractive are the electrochemical properties of the composite $\text{Fe}(\text{Htrz})_3@ \text{SiO}_2$ material, exhibiting highly stable operational stability (i.e., identical voltammetric signals upon multiple successive measurements), contrary to $\text{Fe}(\text{Htrz})_3$ species incorporated by impregnation of the surfactant phase which are found to leach out in solution upon use. Such *in situ* elaborated mesoporous composite made of $\text{Fe}(\text{Htrz})_3$ template strongly immobilized in a silica host is thus promising for bridging the gap between soft and hard functional organic-inorganic materials, which is briefly illustrated here for the mediated detection of hydrogen peroxide thanks to the electrocatalytic properties of the $\text{Fe}(\text{Htrz})_3$ complex, which are maintained even when immobilized in the composite $\text{Fe}(\text{Htrz})_3@ \text{SiO}_2$ film.

Keywords: spin crossover complex, mesoporous silica film, nanocomposite, $\text{Fe}(\text{Htrz})_3$, electrocatalysis.

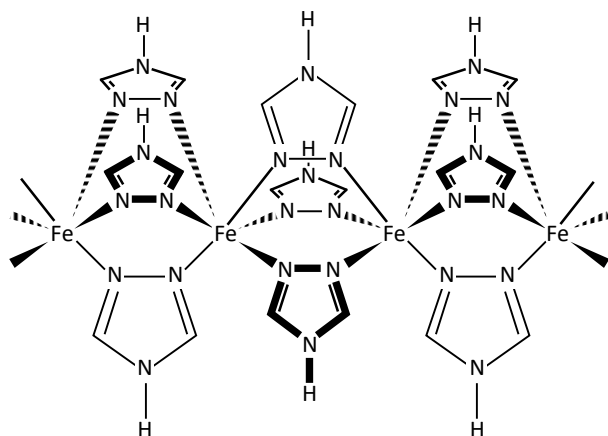
1. Introduction

One of the key scientific questions for chemists of the 21st century is “How far can we push chemical self-assembly?”.¹ Inspired from Nature, molecular self-assembly is ubiquitous in designing complex biological systems and it has emerged in the past decades as an elegant bottom-up method for fabricating nanostructured materials.^{2,3} Self-assembly usually refers to the spontaneous organization of molecular building blocks or nano-objects owing to noncovalent interactions,⁴ giving rise to structurally well-defined ensembles.² Since the first report on ordered mesoporous silicates generated by a surfactant directed cooperative self-assembly approach,⁵ the preparation of nanostructured inorganic solids with organic templates has become a platform for new generations of functional hybrid materials.⁶⁻⁸ Beside the widely used ionic or nonionic surfactants and amphiphilic block copolymers extensively used as templates to fabricate well-defined nanomaterials with controlled structural dimensions and shape,^{6,9-12}

other types of structure-directing agents have appeared in view of extending the characteristics of mesoporous silica-based materials, thus widening the scope of their application. For example, one can cite surfactant/swelling-agent micellar templates for getting ultra-large pores,¹³ the combination of soft and hard templates or the use of solid lipid nanoparticles for the elaboration of hierarchical porous structures,^{14,15} the use of ionic liquids to form mesoporous ionogels,¹⁶ or the resort to functionalized surfactants which may lead to functional hybrid materials in one step.¹⁷ From that last point of view, even if organically functionalized mesoporous silica can be obtained from either post-synthesis grafting or co-condensation using appropriate organosilane reagents or as periodic mesoporous organosilica,^{7,18} a straightforward way to functional mesoporous materials would be via the use of non-surfactant molecular templates that would fill the mesopores while acting as porogen during the formation of the silica network.^{19,20} The spontaneous formation of ordered mesoporous silica using non-surfactant templates remains however highly challenging, especially if wishing to prepare a silica-based materials containing the molecule alone (i.e., without another porogen), as sol-gel processing in the presence of non-templating organic additives usually leads to their molecular dispersion in the silica matrix, resulting in disordered mesoporous materials.²¹ An exception is the particular case of cyclodextrins, which are known to self-assemble and form aggregates in aqueous solutions,²² enabling an ordered aggregation with silica (mostly through wormlike mesopore systems²³) to form functional nanostructures.²⁴ Though not belonging to the surfactant family, it should be emphasized that such cyclic oligosaccharides can be considered as amphiphilic molecules as cyclodextrins are characterized by a hydrophobic interior and a hydrophilic exterior,²⁵ making even more scarce the mesoporous silica-based materials formed from non-surfactant/amphiphilic templates.

Here we would like to evaluate the possible incorporation of a spin crossover complex, $\text{Fe}(\text{Htrz})_3$ (Htrz = 1,2,4,-1*H*-triazole), into a mesoporous silica matrix during its formation. Iron-based spin crossover complexes have received considerable attention due to their numerous potential applications in optical,

electronic, catalysis and/or sensing.²⁶⁻²⁷ However, the design of spin-crossover based devices requires an appropriate processing of the materials at the nanoscale in the form of supported nanostructures, nanoparticles dispersed in soft media, nanocomposites, molecular thin films.²⁸⁻²⁹ Within the whole spin-crossover family of molecular compounds, the Fe(II)-triazole coordination polymers of the general formula $[\text{Fe}(\text{Rtrz})_3]\text{X}_2$ (Rtrz is a functionalized 4-R-1,2,4,5-tetrazole derivative, and X is a counter ion) certainly present the most appealing optical, magnetic, and electronic characteristics for technological applications (i.e. close to room temperature bistability, large hysteresis, ease of chemical preparation and chemical tunability).³⁰ Triazole derivatives are known to coordinate with iron(II) in solution to form coordination polymers, where the iron(II) centers can adopt two different spin states, that is, the low spin (LS) and high-spin (HS) states that are interconvertible upon external stimuli (temperature, pressure, light-irradiation). As recently proved by X-ray crystallography³¹, Fe(II)-triazole systems self-assemble as infinite chains (or finite polynuclear Fe(II) oligomers, e.g. dimers or trimers)³² of Fe(II) cations triply bridged by triazole ligands (scheme 1); this structural connectivity also takes place in solution and metallogels to some extent.^{32,33} The ability to isolate and maintain such linear complexes in appropriate media or nanocomposite would provide interesting functional spin crossover molecular wires. Several strategies based on self-organized molecular assembly have been proposed, such as functionalizing the triazole ligand with long alkyl chain or large lipophilic substituents, or using lipophilic counter-ions to generate metallogels or liquid crystals.³⁴⁻³⁷ These exhibit magnetic and optical properties (and even thermal hysteretic behavior and photofunctionality)³⁸ originating from the parent spin-crossover precursors. Alternatively, nanoparticles (or at least coordination clusters) of Fe(II)-triazole complexes have been incorporated into mesoporous silica-based matrices to obtain monolith or thin film nanocomposites.³⁹⁻⁴² However, while the porosity in terms of pore size distribution and pore surface functionalization can be tuned and controlled, these nanocomposites do not present any ordering or adjustable spatial organization of the confined spin crossover entities.



Scheme 1. Chemical structure of the Fe(II)-triazole coordination polymer (counter-anions are omitted).

Mesoporous materials can be manufactured in several morphologies, but the thin film one offers many advantages in view of insertion into devices for target applications.⁴³ Another important feature is the control of mesopores orientation over a macroscopic scale in order to get well-defined positions of guest molecules and highly controlled molecular events in the channels.⁴⁴ Ordered mesoporous silica thin films are usually prepared by evaporation-induced self-assembly (enabling to tune the final mesostructure by an appropriate control of the experimental conditions used⁴⁵), but getting mesochannels orthogonally oriented onto the underlying support has required the development of more specific methods.⁴⁶⁻⁴⁸ Among them, the electrochemically assisted self-assembly (EASA) approach has proven to be a simple, versatile and fast way to generate vertically aligned mesoporous silica membranes onto electrode surfaces.^{46,49} Such oriented hexagonally packed mesopores offer an ideal configuration for applications (e.g., in the sensors field,^{50,51} where their vertical alignment ensures fast diffusion processes and high sensitivity^{52,53}), as otherwise reported for other types of oriented films (based on mesoporous metal⁵⁴⁻⁵⁶ or metal oxides⁵⁶⁻⁵⁸). They exhibit unprecedented molecular sieving properties for an amorphous film,⁵⁹ along with charge selectivity features,^{60,61} making them very promising for use as permselective or antifouling membranes, for instance.⁶²⁻⁶⁴ They can be obtained in organically-functionalized forms by using organosilane reagents and/or exploiting multi-step click chemistry approaches,⁶⁵⁻⁶⁷ but to date no

attempts to incorporate organo-functional moieties as “simple molecular additives” to the synthesis medium for possible incorporation into such oriented mesoporous films have been made. Otherwise, sol-gel electrodeposition has been applied to the entrapment of large compounds such as redox proteins or enzymes within silica films,^{68,69} but the resulting biocomposite coatings were not ordered at all as these biomolecules are not expected to be involved in self-assembly and mesoporous silica templating.

The aim of the present work is thus to investigate the use of the spin crossover $\text{Fe}(\text{Htrz})_3$ complex (scheme 1) as additive and/or template for the preparation of mesoporous silica thin films by EASA, the ultimate objective being to evidence a real template role of such molecular species in designing ordered composite films containing only the $\text{Fe}(\text{Htrz})_3$ complex in an stable/active form. By varying the amount of $\text{Fe}(\text{Htrz})_3$ in the starting sol solution (in addition to TEOS and CTAB), we will show that low concentrations (≤ 3 mM) ensure to keep a vertically aligned mesostructure with $\text{Fe}(\text{Htrz})_3$ complexes co-incorporated with the surfactant species, whereas larger contents (5 mM) lead to wormlike mesoporous films filled with $\text{Fe}(\text{Htrz})_3$ species that are durably immobilized as a real template in the silica matrix. The film composition and structure are confirmed by XPS, FTIR and TEM. Their electrochemical properties are characterized by cyclic voltammetry, showing remarkable operational stability at high potential scan rates for the wormlike $\text{Fe}(\text{Htrz})_3$ -templated films, which can be exploited in electrocatalysis, for instance.

2. Experimental Section

2.1. Chemicals and reagents

Tetraethoxysilane (TEOS, 98%, Alfa Aesar), ethanol (95-96%, Merck), HCl (37% Riedel de Haen), NaNO_3 (99%, Fluka), cetyltrimethylammonium bromide (CTAB, 99%, Acros), have been used as received. The $\text{Fe}(\text{Htrz})_3$ complex was prepared from $\text{Fe}(\text{BF}_4)_2$ and 1,2,4,1*H*-triazole as previously described.⁴² Indium-tin oxide (ITO) plates (surface resistivity 8-12 Ω) were purchased from Delta Technologies. Analytical grade

ferrocene dimethanol (FcMeOH, Alfa Aesar) was used as redox probes for electrochemical monitoring of mass transport through the films. H₂O₂ (30%, WWR Chemicals) was used for electrocatalytic studies.

2.2. Preparation of the films

The mesoporous silica thin films have been electrochemically generated on ITO electrodes according to the previously reported EASA procedure,^{46,49} which was adapted for incorporating the Fe(Htrz)₃ complex. The starting sol was a hydroalcoholic solution (10 mL H₂O + 10 mL ethanol) containing 100 mM of the silica precursor (TEOS), 32 mM of CTAB as template, 0.1 M NaNO₃ as electrolyte, and variable concentrations of the Fe(Htrz)₃ complex (from 0 to 5 mM). The pH was adjusted to 3 by adding 0.1 M HCl. After a first step of hydrolysis for 2.5h, a cathodic potential of -1.3 V was applied for 20 s to the ITO working electrode (optimized values⁴⁹), leading to the growth of the mesoporous silica or the Fe(Htrz)₃-silica nanocomposite layers. The electrode surface was then thoroughly rinsed with water and aged overnight at 130°C. Extraction of the CTAB was performed by immersing the film electrode in an ethanol solution containing 0.1 M HCl for 15 min.

2.3. Apparatus

All the electrochemical experiments were performed using a μ AutoLab III potentiostat (Eco Chemie) monitored by the GPES software. A three electrode configuration was employed for all measurements, including the electrogeneration, evaluation of the permeability properties, and characterization of the Fe(Htrz)-functionalized silica-based mesoporous films. The voltammetric curves were recorded using a platinum rod as counter electrode, a Ag/AgCl reference electrode (Metrohm) and ITO plates as working electrodes where the hybrid films were deposited. The electrochemically-assisted deposition was carried out using a home-made electrochemical cell with a configuration allowing placing the working electrode at the bottom (see Scheme S1 in Supporting Information). A stainless steel counter electrode and AgCl-coated silver wire pseudo-reference electrode completed the electrochemical setup.

Mesostructure, morphology, and thickness of the films have been analyzed by transmission electron microscopy (TEM) using a ACCEL ARM 200F microscope at an acceleration voltage of 200 kV. X-ray Photoelectron Spectroscopy (XPS) characterizations were performed using a KRATOS Axis Ultra X-ray photoelectron spectrometer (Kratos Analytical, Manchester, UK) equipped with a monochromated AlK α X-ray source ($h\nu = 1486.6$ eV) operated at 150 W. Fourier transform infrared spectroscopy (FTIR) measurements were performed using a Nicolet 8700 apparatus equipped with a diffuse reflectance accessory (Smart Collector).

3. Results and discussion

3.1. Preliminary observations

Figure 1 shows typical cyclic voltammograms recorded for mesoporous silica films prepared from sol solutions containing increasing contents of the Fe(Htrz) $_3$ complex (in addition to TEOS and CTAB). The as-synthesized films revealed distinct behavior depending on Fe(Htrz) $_3$ concentration in the synthesis medium (Fig. 1A): the films obtained from [Fe(Htrz) $_3$] up to 2 mM are characterized by rather ill-defined signals with almost no reversibility whereas the curves observed for more concentrated media ([Fe(Htrz) $_3$] ranging from 3 to 5 mM) gave rise to well-defined peaks on both forward and reverse scans. After treatment in HCl/ethanol (which is expected to remove the CTAB template from the film⁴⁹), the situation was significantly different, with still well-defined responses for the more concentrated films but no noticeable signals for the electrodes covered with nanocomposites prepared from [Fe(Htrz) $_3$] lower than 2 mM (Fig. 1B). It seems therefore that the Fe(Htrz) $_3$ complexes incorporated into the materials from the most diluted sol solutions are washed out of the films along with the surfactant template while those entrapped from the most concentrated sol solutions survive the solvent extraction step. In this latter case, the intensity of the voltammetric signals (which can be related to the amount of Fe(Htrz) $_3$ in the film) is proportional to the Fe(Htrz) $_3$ concentration used to prepare the films. These preliminary results (Fig. 1) demonstrate the successful incorporation of Fe(Htrz) $_3$ complexes into the mesoporous

silica films, most probably due to favorable electrostatic interactions between the negatively charged silica precursors and the positive complex, but they also suggest significant behavioral differences depending on the amount of entrapped $\text{Fe}(\text{Htrz})_3$ species.

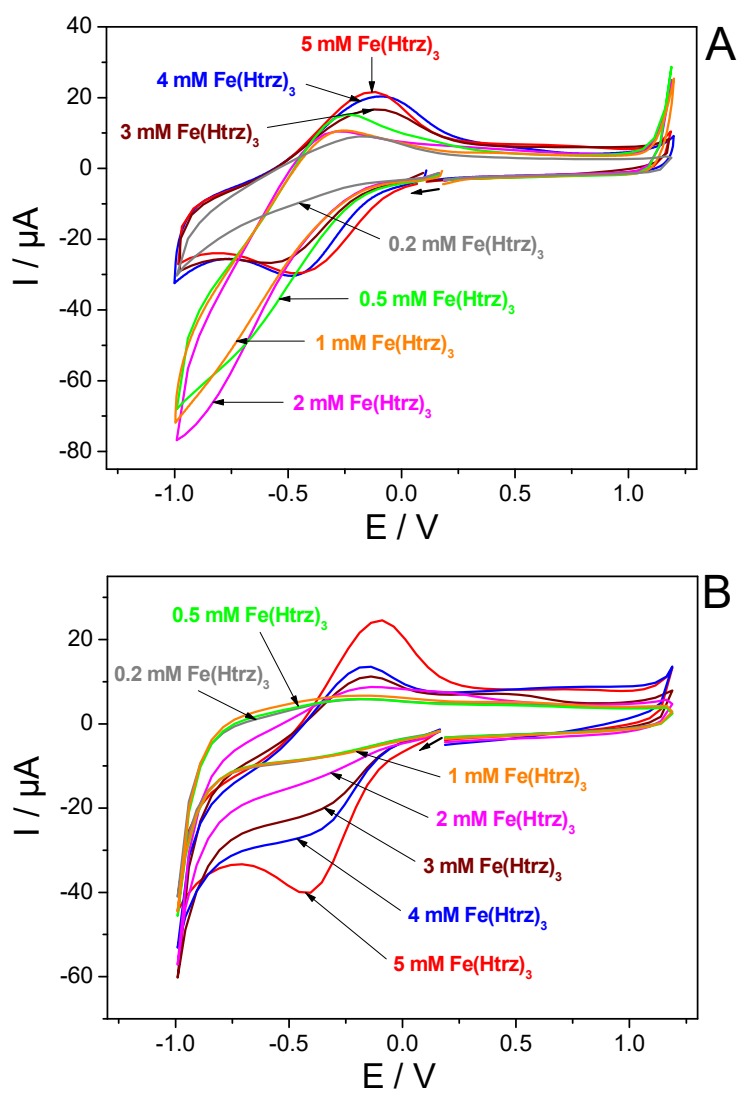
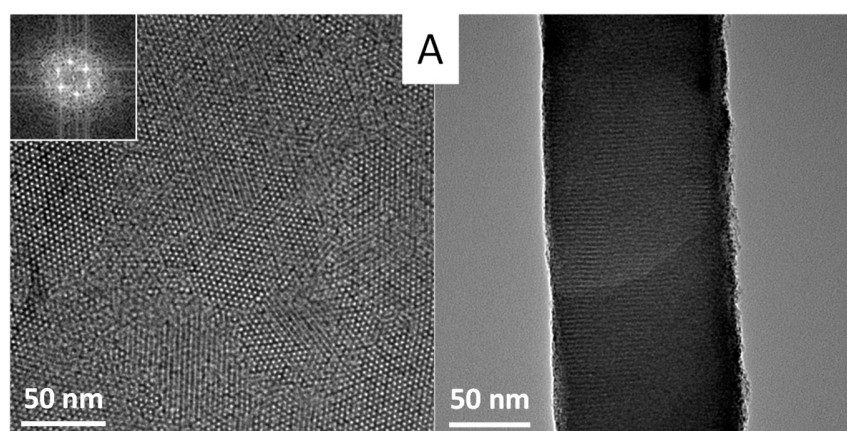


Figure 1. Cyclic voltammograms recorded at 0.5 V s^{-1} in 0.1 M NaNO_3 aqueous solution using mesoporous silica film modified ITO electrodes prepared from a starting sol containing increasing concentrations of $\text{Fe}(\text{Htrz})_3$ complex (from 0.2 to 5 mM), respectively before (A) and after film treatment in 0.1 M HCl in ethanol (B).

3.2. Structural characterization and permeability properties of the films

From the EASA procedure used to prepare the films,^{46,49} one already knows that their expected structure is made of well-organized and hexagonally-packed mesopore channels vertically aligned onto the electrode surface, which is confirmed here from TEM micrographs and the electron diffraction pattern (see top and cross-section views Fig. S1 in Supporting Information). This oriented mesostructure is maintained up to 3 mM Fe(Htrz)₃ in the synthesis medium (Fig. 2A-C), as also supported by GISAX characterization (see Fig. S2 in Supporting Information), suggesting that the incorporation of few amounts of this complex does not affect the final mesostructured (yet with some quality loss for the sample prepared from 3 mM Fe(Htrz)₃, see Fig. 2C). However, larger Fe(Htrz)₃ contents led to clearly less ordered but still regular wormlike mesostructures (see, e.g., Fig. 2D for a film prepared from 5 mM Fe(Htrz)₃), yet uniformly deposited over the whole electrode surface and keeping constant thickness over the whole membrane area; the wormlike structure can be also evidenced by XRD (see Fig. S2 in Supporting Information), giving rise to a lattice parameter of 4.7 nm (consistent with TEM). One can even notice some stigmata of the vertical orientation in these highly loaded films; see top of cross-section view in Fig. 2D). The film thickness is independent on the Fe(Htrz)₃ concentration in the sol solution (i.e., 110±5 nm), indicating that the rate of film growth is not affected by the presence of the complex.



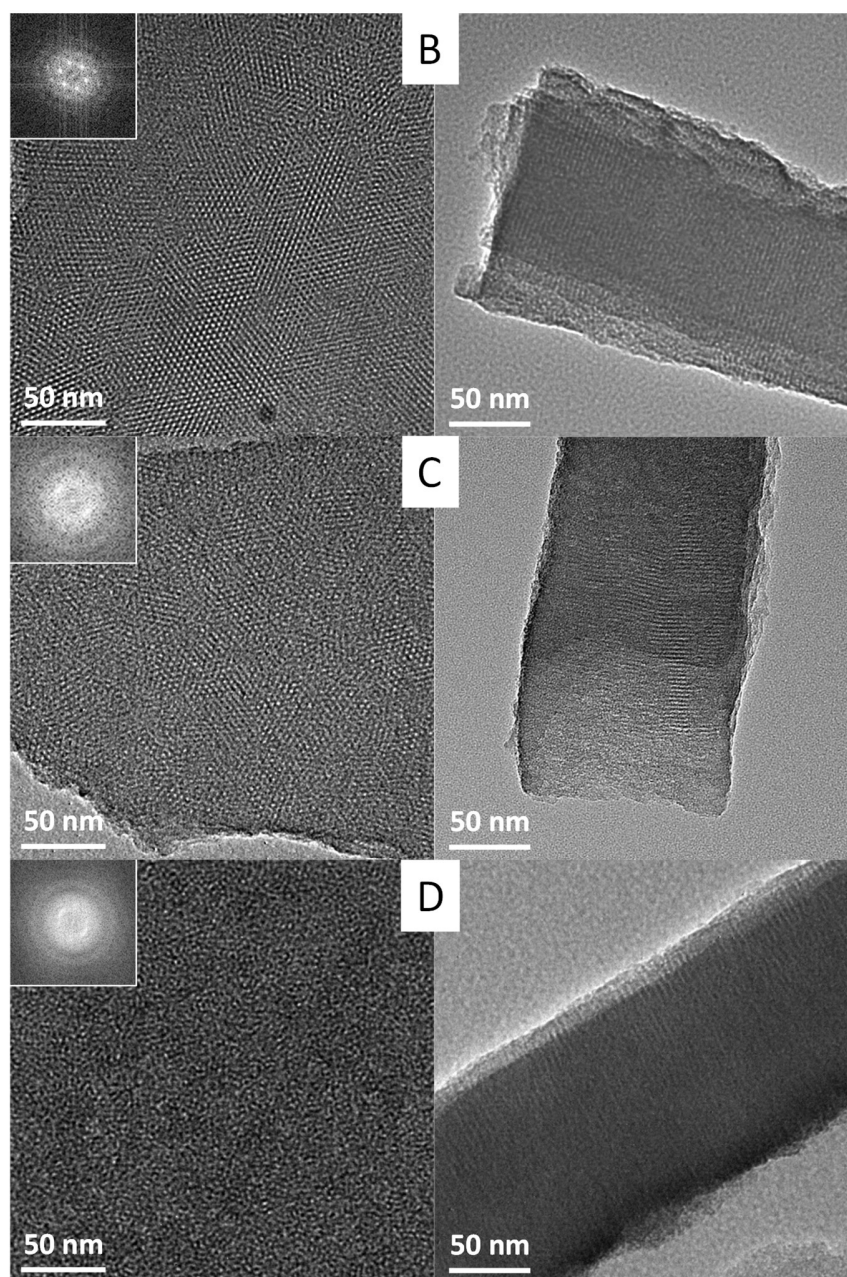


Figure 2. TEM micrographs (top views on the left and cross-sections on the right) of mesoporous silica films prepared by EASA from a starting sol containing TEOS and CTAB in the presence of increasing concentrations of $\text{Fe}(\text{Htrz})_3$ complex: 0.5 mM (A), 1 mM (B), 3 mM (C) and 5 mM (D). Electron diffraction patterns are also shown on top view micrographs.

Permeability measurements can bring additional information on the film properties, notably by comparing data obtained before and after treatment in HCl/ethanol (Fig. 3). Electrodes covered with template-based mesoporous silica films in general,^{70,71} and the oriented ones in particular,^{61,71} have typical electrochemical signatures when using selected redox probes in solution. This is illustrated in part A of the figure for the ferrocenedimethanol probe ($\text{Fc}(\text{MeOH})_2$), showing before template removal a reversible signal around +0.5 V corresponding to the $\text{Fc}(\text{MeOH})_2/\text{Fc}(\text{MeOH})_2^+$ system solubilized in the surfactant phase and, after CTAB extraction the voltammetric response typical for $\text{Fc}(\text{MeOH})_2$ on ITO at about +0.3 V because the probe is now able to cross the film to reach the electrode surface (peak currents are even slightly larger for the film electrode than on bare ITO because $\text{Fc}(\text{MeOH})_2^+$ cations are likely to be accumulated onto the negatively charged silica walls). The potential shift observed for the film before template extraction is explained by the stabilization of the neutral $\text{Fc}(\text{MeOH})_2$ probe in the surfactant phase (making it more difficult to be oxidized into $\text{Fc}(\text{MeOH})_2^+$ that is repelled by the cationic surfactant, in agreement with previous observations made for the electrochemistry of ferrocene derivatives in micellar media⁷²). We have thus repeated these experiments using the film electrodes containing various $\text{Fe}(\text{Htrz})_3$ contents, respectively before (Fig. 3B) and after treatment in HCl/ethanol (Fig. 3C), which is in principle likely to remove the template from the films. For as-synthesized films, the voltammetric response to $\text{Fc}(\text{MeOH})_2$ probe was dramatically decreased or even totally suppressed (Fig. 3B). Only small and ill-defined signals were observed with films prepared from $\text{Fe}(\text{Htrz})_3$ concentrations lower than 2 mM. This indicates that the presence of $\text{Fe}(\text{Htrz})_3$ complex in the mesoporous film restricts or even totally prevents the redox probe from reaching the underlying electrode surface, suggesting that few or no $\text{Fc}(\text{MeOH})_2$ species are likely to be solubilized in the template phase containing increasing contents of $\text{Fe}(\text{Htrz})_3$ complex. The absence of response also indicates that the nanocomposite films are well recovering the whole electrode surface area and that they are crack-free (otherwise, the probe would have been able to enter the defects and give a response when reaching the electrode).

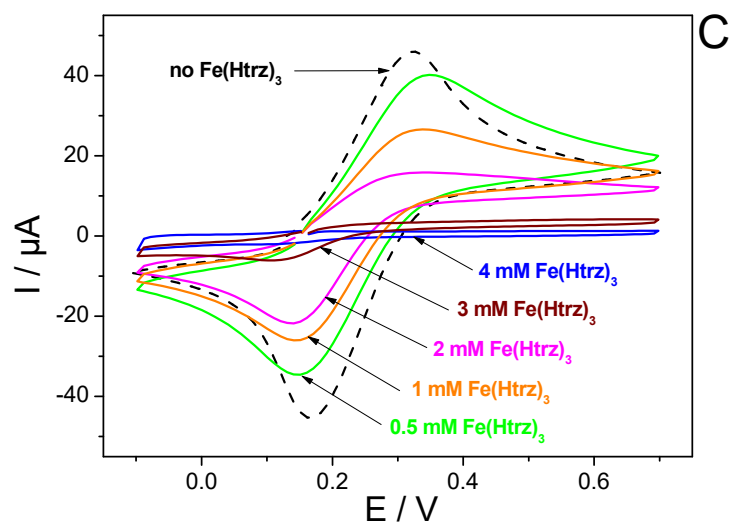
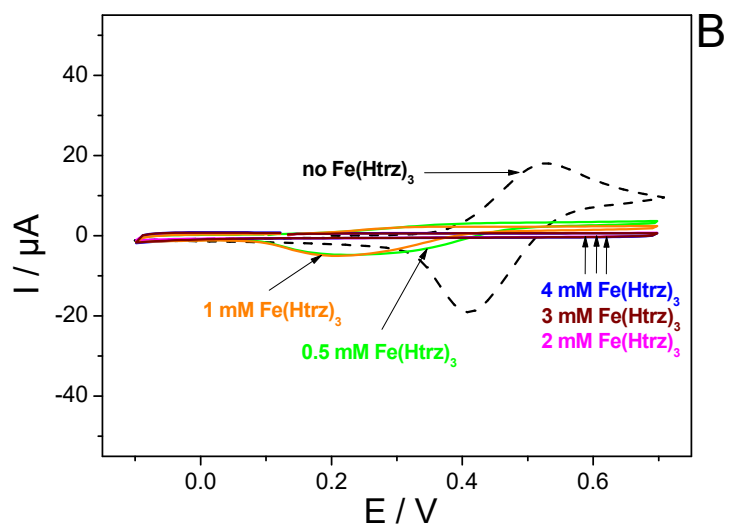
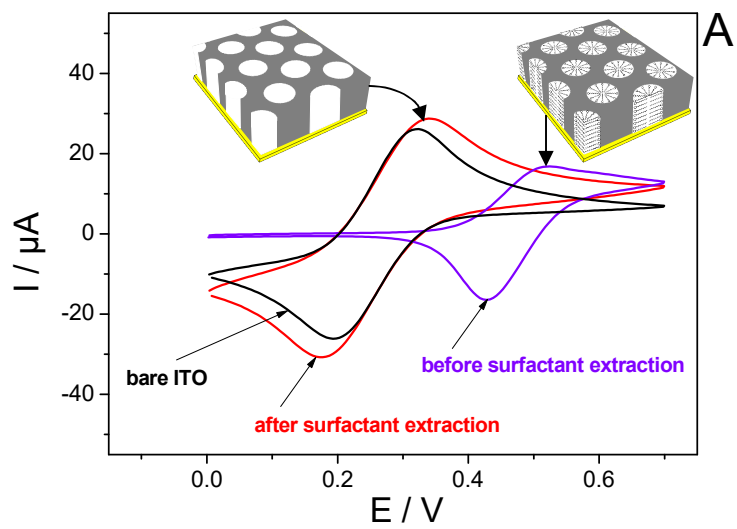


Figure 3. (A) Cyclic voltammograms recorded at 100 mV s^{-1} in 1 mM Fc(MeOH)_2 ($+0.1\text{ M NaNO}_3$) aqueous solution using either bare ITO or ITO electrodes covered with an oriented mesoporous silica film (prepared by EASA from a starting sol containing only TEOS and CTAB), respectively before and after surfactant removal. (B,C) Cyclic voltammograms recorded in the same conditions as in (A) but using mesoporous silica films modified ITO electrodes prepared from the same starting sol as above to which various concentrations of Fe(Htrz)_3 complex (from 0.5 to 4 mM) have been added, respectively before (B) and after film treatment in 0.1 M HCl in ethanol (C).

After treatment in HCl/ethanol, usually applied to extract the surfactant template and make the mesopore channels open to free diffusion of the probe (as for undoped mesoporous silica film, see red curve on Fig. 3A), the Fe(Htrz)_3 -doped films behaved differently as a function of the Fe(Htrz)_3 content (Fig. 3C). For the films prepared at Fe(Htrz)_3 concentrations up to 3 mM , surfactant template removal seems to be effective as the Fc(MeOH)_2 probe gave rise to well-defined voltammetric signals at about $+0.3\text{ V}$. Yet, their intensity is decreasing when passing from low to high Fe(Htrz)_3 contents, suggesting increasingly limited diffusion rates for the probe through the nanochannels. Such restricted mass transport, which was already observed with mesoporous silica films grafted with increasing amounts of organo-functional groups,⁷³ is thought to be due to residual Fe(Htrz)_3 complexes that were not removed from the film during CTAB removal by solvent extraction (consistent with results of Fig. 1B) thus occupying some space in the mesopore channels and impeding somewhat the diffusion of Fc(MeOH)_2 . Another argument supporting the restricted electrochemical response of Fe(Htrz)_3 -doped films is the larger anodic-to-cathodic peak potential separation (by ca. 40 mV) relative to the unmodified mesoporous silica film. Even more surprising is the complete blocking of films prepared from Fe(Htrz)_3 concentrations larger than 3 mM (see, e.g., blue curve in Fig. 3C, corresponding to 4 mM Fe(Htrz)_3), suggesting that the classical HCl-ethanol treatment for surfactant extraction is ineffective for the removal of the complex from such highly concentrated films. This suggests a good stability of the

incorporated Fe(Htrz)₃ species in the hybrid material, which is thought to be due to a combination of effects (triazole ligand-driven formation of a coordination polymer, physical entrapment of polymer chains in the mesopore channels, favorable electrostatic interactions between the positive complexes and negative silica walls). The only way to deeply unclog the mesopores and reveal the film permeability to the redox probe was to calcine the nanocomposite material (see Fig. S3 in Supporting Information), yet with some iron remaining in the matrix (≈ 1 %, as revealed by EDX analysis). Note that treatment in a more concentrated acid solution (i.e., 1 M HCl) also resulted in some film permeability but without removing all complex species from the material (see Fig. S4 in Supporting Information). This unexpected behavior might be of interest in view of confining durably such spin crossover complex into a mesoporous silica matrix. In order to understand better these phenomena, spectroscopic analyses have been performed, aiming at the evaluation of mesopore composition respectively before and after template extraction.

3.3. Mesopores composition and effect of solvent extraction on template removal

XPS was first used to investigate the surface composition and the chemical environment of the elements likely to be part of the Fe(Htrz)₃-doped mesoporous silica films. XPS survey spectra (not shown) indicate the presence of C_{1s}, O_{1s}, N_{1s}, Si_{2p} and Fe_{2p} signals, the intensity of which evolving with the amount of Fe(Htrz)₃ complex and varying upon treatment in HCl/ethanol (see Table S1 in Supporting Information). The most important conclusions can be drawn from the analysis of narrow scan regions corresponding to N_{1s} and Fe_{2p} signals (Fig. 4). From the analysis of Fe_{2p} core level spectra (Fig. 4A), one can see a gradual decrease in signal intensity for both 2p_{3/2} and 2p_{1/2} peaks respectively located at the binding energies 711.1 and 724.5 eV (corresponding to a 2p_{3/2}-Fe 2p_{1/2} splitting of 13.4 eV, along with their characteristic satellites at a distance of 5 eV, which are consistent values for Fe-1,2,4-triazole compounds⁷⁴). After HCl/ethanol treatment, almost no change was observed for the sample prepared from 5 mM Fe(Htrz)₃ (decrease in the Fe atomic content within the margin of error), suggesting no significant loss of the

complex upon solvent extraction, whereas the films prepared from $\text{Fe}(\text{Htrz})_3$ concentrations lower than 2-3 mM suffered from dramatic leaching and even complete removal of $\text{Fe}(\text{Htrz})_3$ species from the mesoporous silica material. These data are in agreement with preliminary electrochemical observations (Fig. 1B). This is also supported by C_{1s} signals showing notably a line at 288.8 eV (corresponding to N-C=N centers in the triazole ring^{75,76}) which remained intact after solvent extraction for the 5 mM sample, whereas the lines characteristic of the CTAB template (C-C at 284.5 eV and C-N at 286.0 eV) dramatically decreased upon solvent extraction of the films prepared from lower $\text{Fe}(\text{Htrz})_3$ concentrations (see Fig. S5 in Supporting Information), but such data have to be taken with great care because of the existence of carbon-containing contamination and residual ethoxy groups resulting in C_{1s} peaks at similar binding energies.^{77,78} In addition, considering previous XPS studies involving iron, the $2p_{3/2}$ peak for high-spin Fe(III) and Fe(II) compounds is broadened compared to metallic Fe^0 or low-spin Fe(II)⁷⁹ due to the inclusion of electrostatic interactions, spin-orbit coupling between the 2p core hole and unpaired 3d electrons of the photoionized Fe cation and crystal field interactions.^{80,81} The $2p_{3/2}$ peaks from low-spin Fe(II) compounds display no multiplet interactions because all six 3d electrons are spin paired.⁸² The broadened peaks observed on the Fe_{2p} spectra in addition to the binding energies observed at 711.1 and 724.5 eV seem to be in good agreement with the presence of Fe(III) in the mesoporous films (despite the iron-triazole complex introduced in the starting sol solution used to prepare the films is a low spin Fe(II) complex). This suggests that an oxidation of Fe(II) into Fe(III) centers takes place during the generation of the films, and this will be demonstrated and discussed later on (see beginning of Section 3.4). From Fe_{2p} signals, one can also see some correlation between the iron content in the mesoporous films with the $\text{Fe}(\text{Htrz})_3$ concentration in the starting sol (see Table S1 in Supporting Information).

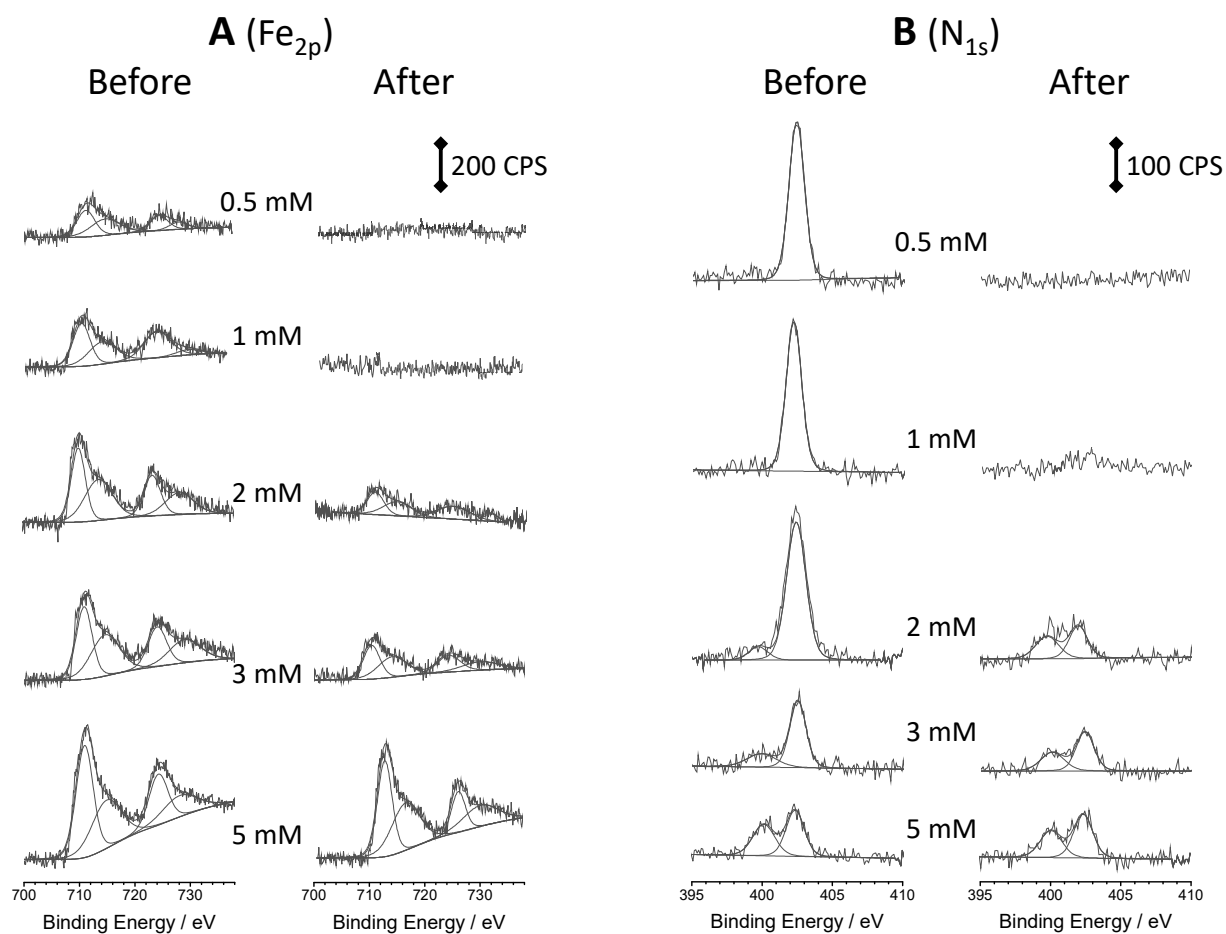


Figure 4. High-resolution XPS spectra for (A) iron ($2p$) and (B) nitrogen ($1s$) obtained using mesoporous silica films modified ITO electrodes prepared from a starting sol containing TEOS, CTAB, and various concentrations of $Fe(Htrz)_3$ complex (from 0.5 to 5 mM), respectively before and after film treatment in 0.1 M HCl in ethanol.

The analysis of N_{1s} core level spectra (Fig. 4B) further confirms the above observations. At low $Fe(Htrz)_3$ contents, the only visible contribution to the N_{1s} core level is due to the presence of the surfactant template, appearing in the form of a single peak located at 402.4 eV (assigned to the ammonium groups originating from CTAB).⁸³ This signal disappeared after HCl/ethanol treatment, confirming surfactant

removal (as for unmodified mesoporous silica films⁸⁴). Increasing the Fe(Htrz)₃ content at 2-3 mM and above led to considerable decrease of this signal with concomitant growth of an additional peak at 400.1 eV which can be ascribed to the triazole moieties.^{74,76} For the highest Fe(Htrz)₃ content (5 mM), its intensity remained almost unchanged, confirming the strong binding of the complex to the mesoporous silica film, which acted thus as a real template during film growth owing to favorable electrostatic interactions between the cationic complex and the negatively charged silica precursors (electrostatic attraction has been also claimed for Fe(Htrz)₃ in Nafion,⁸⁵ for instance). The residual N_{1s} contribution at 402.4 eV (with same intensity before and after HCl/ethanol treatment) cannot be unambiguously explained as it can be due to the amine functions of the triazole ring interacting with the silanol groups (via H-bonding or protonation, as reported for cyclam-functionalized silica materials⁸⁶) or to some remaining CTA⁺ species not washed out by solvent extraction and likely to act therefore as co-template.

FTIR analyses were also performed to confirm XPS observations, notably to check if information gathered from surface composition is also true for the bulk film. The results (see Fig. S6 in Supporting Information) indicate the presence of Fe(Htrz)₃ (from typical vibrations of =C-H, -N-H, -C=N and -N=N groups^{87,88}) with no or negligible amount of CTAB in the sample prepared from 5 mM of the complex, which remained in the film after HCl/ethanol treatment, whereas only the surfactant template was noticeable in the film generated from 0.5 mM Fe(Htrz)₃ and it was completely removed after solvent extraction. This supports conclusions made from XPS data. FTIR results also show the absence of signal in the region 3300-3500 cm⁻¹ corresponding to OH groups (from silanol or water) when the film contained CTAB as the template (the signal only occurred after HCl/ethanol treatment), while it was clearly visible for the sample obtained when Fe(Htrz)₃ acted as the template due to its more hydrophilic character.

From all the above results, one can thus clearly distinguish two cases: the nanocomposite films exhibiting a wormlike mesostructure filled with Fe(Htrz)₃ species that are durably immobilized as a real template in the silica matrix (i.e., as generated from a sol solution containing a high concentration of the iron triazole

coordination polymer), and the vertically aligned hexagonal mesostructure with $\text{Fe}(\text{Htrz})_3$ complexes co-incorporated with the surfactant species (as obtained at $\text{Fe}(\text{Htrz})_3$ contents ≤ 3 mM) which suffer from important leaching of $\text{Fe}(\text{Htrz})_3$ species from the film upon solvent extraction. Note that durable immobilization of the complex does not mean an improved chemical stability of the hybrid material in comparison to pure mesoporous silica films, as the silica walls are still constituted of amorphous silica gel which can suffer from some degradation upon prolonged use in aqueous media, especially at high pH values. In the following section, we will focus only on the film electrode prepared from 5 mM $\text{Fe}(\text{Htrz})_3$ in order to point out the possible interest of such strongly immobilized complex as an electroactive template for electrocatalytic purposes.

3.4. Electrochemical characterization and electrocatalytic properties of immobilized $\text{Fe}(\text{Htrz})_3$

It appears from preliminary electrochemical experiments (Fig. 1B) and Fe_{2p} XPS data (Fig. 4A) that the immobilized $\text{Fe}(\text{Htrz})_3$ complex in the mesoporous silica material is in the form of Fe(III) although the Fe(II) coordination polymer was used in the synthesis medium. The explanation of such unexpected observation has to be found in the film generation procedure by EASA involving a potential-driven pH increase at the electrode/solution interface (i.e., to induce the condensation of silica precursors at pH above 8)^{89,90} and taking into account the pH-dependent chemistry of $\text{Fe}(\text{Htrz})_3$ and its possible oxidation.^{41,91} This is confirmed from cyclic voltammetry experiments performed with the Fe(II) form of the complex in aqueous solution at distinct pH (see Fig. S7 in Supporting Information) showing that it is intact at pH 3.5 (colorless and oxidizable species) whereas the solution turned yellowish at pH 9 due to the chemical oxidation of Fe(II) into Fe(III), resulting in a well-defined cathodic response. One can therefore conclude that the $\text{Fe}(\text{Htrz})_3$ complex acting as template during the growth of the mesoporous silica films is in its oxidized Fe(III) form, as a consequence of the electrochemical reduction of water leading to the production of OH^- species at the vicinity of the electrode surface in the EASA process.^{46,49}

Figure 5 depicts cyclic voltammograms of the film electrode prepared from 5 mM Fe(Htrz)₃ as recorded at various potential scan rates (Fig. 5A) and under multiple successive cycling conditions at the same scan rate (Fig. 5B). This latter shows remarkable operational stability (no noticeable change in peak currents), which is rather unique for redox species weakly bonded/entrapped in a porous silica matrix confined to an electrode surface for which significant amounts of the electroactive probes are usually lost in solution upon electrochemical excitation, resulting in signals of lower intensity.^{92,93} This is advantageous compared to organic-inorganic hybrid films elaborated from (sometimes sophisticated) covalent binding strategies to ensure durable immobilization of guest species in mesoporous silica films,^{67,93-95} as the present method operates on the basis of a simple and single-step growth of the nanocomposite material. The operational stability extended up to high potential scan rates (>5 V s⁻¹), yet becoming slightly less reversible, while potential scan rates lower than 100 mV s⁻¹ resulted in the progressive decrease in cathodic peak currents with concomitant vanishing of the anodic counterparts on scan reversal (see Fig. S8 in Supporting Information) suggesting possibly lower affinity of the Fe(II) form of the complex for the mesoporous silica matrix. The voltammetric signals are located at -0.35 V vs. Ag/AgCl, with cathodic-to-anodic peak potential difference equal to 0.21 V for potential scan rates up to 400 mV s⁻¹ and increasing somewhat above (see Fig. S8 in Supporting Information), and both cathodic and anodic peak currents are directly proportional to the potential scan rate (see inset in Fig. 5A) indicating a thin layer behavior (i.e., all electroactive species in the film are transformed during the scan, without diffusional restrictions). The fact that the thin layer behavior is maintained at high scan rates (far beyond 1 V s⁻¹) and the good stability of current responses upon multisweep are indicators of the exceptional performance of such films for which the Fe(Htrz)₃ coordination polymer not only plays the role of template but also contributes to stabilize the complex species in an active form in the hybrid nanocomposite. It was not the case of previously reported electroactive guests anchored into mesoporous silica films (which were usually characterized by diffusion-controlled charge transfer),^{93,96} for which dramatic decrease in current

responses were observed (e.g., 70% drop in peak currents after 2 h in blank electrolyte for a mesoporous silica film doped with electrostatically-bound $[\text{Ru}(\text{bpy})_3]^{2+}$ species).⁹⁶

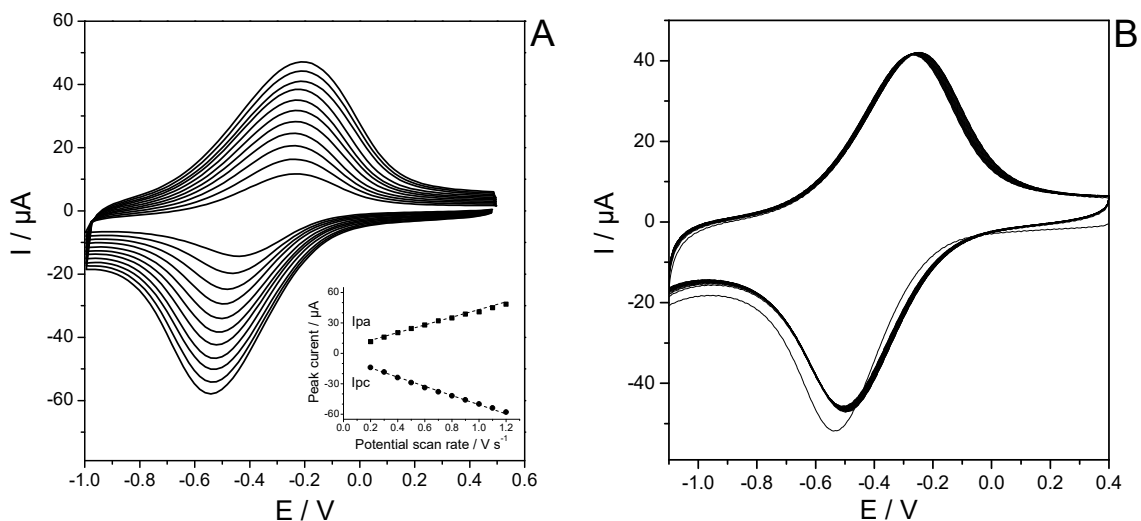


Figure 5. (A) Cyclic voltammograms recorded at various potential scan rates (in the 0.2 to 1.2 V s^{-1} range) in 0.1 M NaNO_3 aqueous solution using a mesoporous silica film modified ITO electrode prepared from $5 \text{ mM Fe}(\text{Htrz})_3$ complex (after film treatment in 0.1 M HCl in ethanol); the variation of peak currents with potential scan rate is shown in the inset. (B) 20 consecutive cyclic voltammograms recorded at 1 V s^{-1} using the same electrode in the same medium as in (A).

Quantitative evaluation of the amount of $\text{Fe}(\text{Htrz})_3$ complex in the film can be achieved from the integration of peak currents in Fig. 5, leading to a charge of ca. $27 \mu\text{C}$, corresponding to $2.8 \times 10^{-10} \text{ mol Fe}(\text{Htrz})_3$, which corresponds to a surface concentration of $\Gamma = 1.4 \times 10^{-9} \text{ mol cm}^{-2}$ (geometric surface area of the electrode = 0.196 cm^2). Taking into account the film diameter (5 mm), thickness (110 nm) and density ($\sim 0.8 \text{ g cm}^{-3}$ for MCM-41⁹⁷), this led to an estimated value of $1.6 \times 10^{-4} \text{ mol g}^{-1} \text{ Fe}(\text{Htrz})_3$ in the film, if assuming that all of them are electroactive (i.e., a reasonable hypothesis for such species confined in the mesopore channels for which the electron transfer mechanism should be the electron hopping between adjacent $\text{Fe}(\text{Htrz})_3$ moieties). Considering the pores density for such films prepared by EASA

(i.e., 75 000 pores μm^{-2} ,⁴⁶ which is also consistent with the top TEM view on Fig. 2D for the wormlike mesostructure) and the surface concentration determined above from voltammetry ($\Gamma = 1.4 \times 10^{-9}$ mol cm^{-2} , corresponding to 8.4×10^{14} molecule cm^{-2}), one can estimate roughly an amount of 110-120 complex units per mesopore, which is compatible with a coordination polymer made of $\text{Fe}(\text{Htrz})_3$ complexes having a length of the same order of magnitude as the film thickness (assuming a complex size of about 1 nm in diameter, as estimated from XRD data). This suggests the filling of all mesopore channels over the whole film thickness and supports further the idea of a template role played by $\text{Fe}(\text{Htrz})_3$ in the mesoporous silica film formation. The direct electron transfer is not possible due to the insulating character of the silica walls, but the high density of $\text{Fe}(\text{Htrz})_3$ complexes very close to each other in the film (i.e., 5 times more than the maximum amount of ferrocene groups that can be covalently-bonded to a similar mesoporous silica film,⁶⁶ for instance) enables effective electron hopping-based charge transfer. Just to illustrate the potential interest of nanocomposite mesoporous films made of a supramolecular electroactive template such as the $\text{Fe}(\text{Htrz})_3$ -based coordination polymer, we provide here a preliminary investigation of their electrocatalytic behavior towards the reduction of hydrogen peroxide. In the presence of H_2O_2 , the reversible signal characteristic of the immobilized $[\text{Fe}(\text{Htrz})_3]^{3+/2+}$ system changed significantly, showing an increase in the intensity of the cathodic peak while the anodic signal almost disappeared (see Fig. S9 in Supporting Information). This is due to the electrocatalytic reduction of H_2O_2 by the electrogenerated $[\text{Fe}(\text{Htrz})_3]^{2+}$ species which are thus no more available to be reoxidized on scan reversal. This can be exploited for the amperometric detection of H_2O_2 , by applying a constant potential (i.e., -0.4 V) to the electrode placed in a stirred electrolyte solution to which increasing concentrations of H_2O_2 are added, and measuring the resulting current responses as depicted in Figure 6. As shown, no detectable response was observed at bare ITO because the direct reduction of H_2O_2 requires more cathodic potential values, whereas well-defined current jumps occurred upon injections of H_2O_2 aliquots of increasing concentrations when using a $\text{Fe}(\text{Htrz})_3$ -doped mesoporous silica film electrode (Fig. 6A).

Comparing the curves obtained from film electrodes prepared from either 3 mM or 5 mM Fe(Htrz)₃ in the synthesis medium (Fig. 6B) reveals that both exhibited an electrocatalytic response to H₂O₂, but the sensitivity obtained with the 5 mM film was larger than for the 3 mM film, confirming the advantages offered by the highly loaded material. The responses were fast, reaching steady-state in few seconds (i.e., >90% of the signal obtained after 3 and 5 s, respectively for films prepared from 5 and 3 mM Fe(Htrz)₃). Focusing on the most sensitive film (generated using 5 mM Fe(Htrz)₃), a linear response was observed in the H₂O₂ concentration range from 1 to 160 μM (see inset in Fig. 6B).

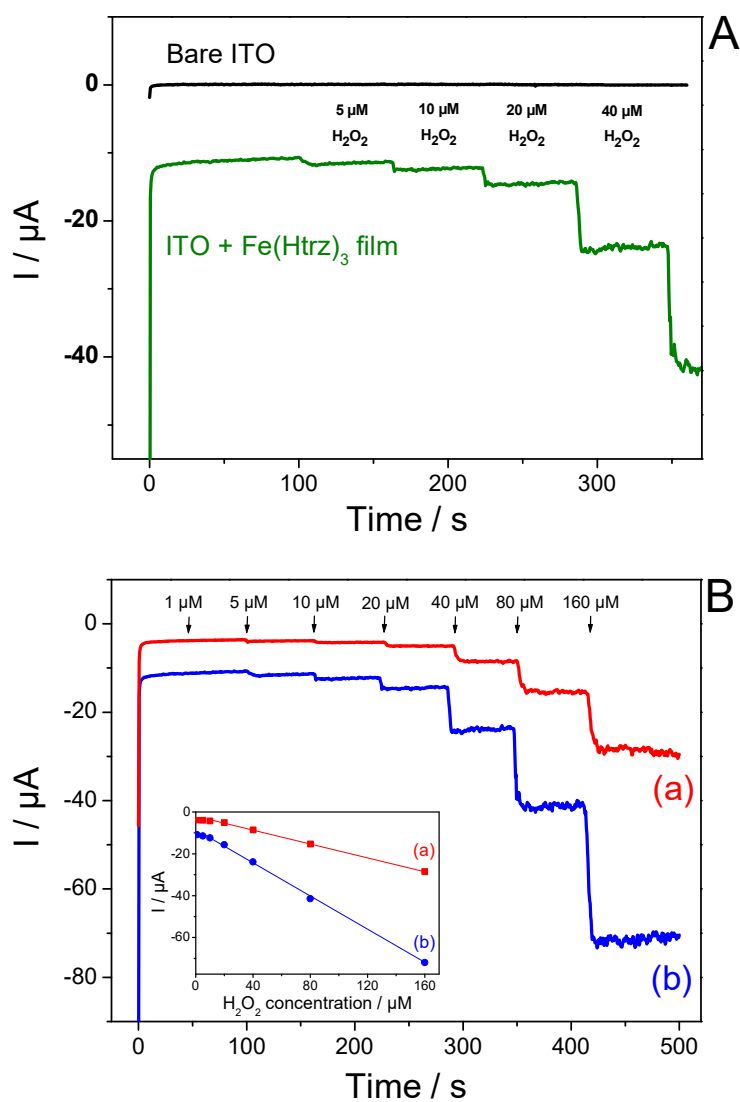


Figure 6. Amperometric responses recorded at bare ITO or using ITO electrodes modified with mesoporous silica films prepared from a starting sol containing TEOS, CTAB, and Fe(Htrz)₃ complex (at 3 or 5 mM), to the addition of increasing concentrations of H₂O₂ (in a stirred aqueous solution of 0.1 M NaNO₃) at an applied potential of -0.4 V: (A) comparison of bare ITO and the film electrode prepared from 5 mM Fe(Htrz)₃; (B) calibration data (amperometric curves and plot of steady-state currents vs. [H₂O₂] in inset) obtained for H₂O₂ in the 1-160 μM concentration range using film electrodes prepared from (a) 3 mM and (b) 5 mM Fe(Htrz)₃.

4. Conclusions

Using a coordination polymer as template, we have designed a general one-step elaboration procedure of mesoporous silica composite thin films based on electrochemically assisted self-assembly. Depending on the concentration of the templating spin-crossover Fe(Htrz)₃ coordination polymer in the starting sol, two distinct situations have been reached. For low Fe(Htrz)₃ concentration (≤ 3 mM), the vertically aligned mesostructure is formed and Fe(Htrz)₃ complexes are co-incorporated with the surfactant species, but most of them are leached out from the film upon surfactant extraction. On the contrary, for high Fe(Htrz)₃ concentration (typically 5 mM), a wormlike mesoporous film is obtained in which Fe(Htrz)₃ species are strongly immobilized within the silica matrix, acting as a novel type of structure-directing agent. For the optimized situation, a density of Fe(Htrz)₃ complexes as high as 1.6×10^{-4} mol g⁻¹ has been estimated, roughly corresponding to an amount of 110 complex units per mesopore channel. This enables efficient electron-hopping charge transfer through the entire film thickness. As a consequence, the resulting Fe(Htrz)₃@SiO₂ composite offers remarkable electrochemical properties, characterized by high operational stability, maintained at high scan rates with a good stability of current response upon multisweep. The potential interest of the composite has been illustrated through its electrocatalytic performance towards the detection of hydrogen peroxide.

These results pave the way to the design of new functional and multifunctional silica composite films, using coordination polymers with appealing physical properties (magnetic, optical, electronic) as template. The synthesis method appears to be very simple and versatile, and optimizing the elaboration conditions could lead to improving the control of the mesostructuration level and pore orientation to get functional molecular entities durably confined in an attractive geometry for applications. One can expect the use of other coordination polymers as template to get in a single step other kinds of organic-inorganic hybrids exhibiting new or improved properties (not only the electrochemical ones) and we are also confident that spin cross-over characteristics of such immobilized iron-triazole complexes might be exploited in near future.

Acknowledgments

Financial supports from the CNRS, the French PIA project "*Lorraine Université d'Excellence*" (reference ANR-15-IDEX-04-LUE) and the CPER (program *SusChemProc*) are acknowledged. We also thank Jaafar Ghanbaja for TEM imaging, Aurélien Renard for recording XPS spectra, and Lionel Richaudeau for GISAXS measurements. SA acknowledges a PhD fellow from the *Université de Lorraine*.

Supporting Information description

Scheme of the electrochemical cell used for film preparation, TEM of unmodified mesoporous silica film, GISAXS of the films, permeability data after film calcination and treatment in 1 M HCl, quantitative XPS data (film composition as a function of Fe(Htrz)₃ concentration), additional characterization data (C1s XPS spectra, FTIR spectra, respectively before and after treatment with ethanol/HCl), pH effect on CV of Fe(Htrz)₃ complex in solution, additional CV curves for Fe(Htrz)₃-modified films at various scan rates, CV characterization of the electrocatalytic detection of hydrogen peroxide at the modified electrode.

References

1. Service, R. F. How Far Can We Push Chemical Self-Assembly? *Science* **2005**, 309, 95.
2. Whitesides G. M.; Mathias J. P.; Seto C. T. Molecular Self-Assembly and Nanochemistry: a Chemical Strategy for the Synthesis of Nanostructures. *Science* **1991**, 254, 1312-1319.
3. Lin, Y.; Boker, A.; He, J.; Sill, K.; Xiang, H.; Abetz, C.; Li, X.; Wang, J.; Emrick, T.; Long, S.; Wang, Q.; Balazs, A.; Russel, T. P. Self-Directed Self-Assembly of Nanoparticle/Copolymer Mixtures. *Nature* **2005**, 434, 55-59.
4. Whitesides G. M.; Grzybowski B. Self-Assembly at All Scales. *Science* **2002**, 295, 2418-2421.
5. Kresge, C. T.; Leonowicz, M. E.; Roth, W. J.; Vartuli, J. C.; Beck, J. S. Ordered Mesoporous Molecular Sieves Synthesized by a Liquid-Crystal Template Mechanism. *Nature* **1992**, 359, 710-712.
6. Wan, Y.; Zhao, D. On the Controllable Soft-Templating Approach to Mesoporous Silicates. *Chem. Rev.* **2007**, 107, 2821-2860.
7. Hoffmann, F.; Cornelius, M.; Morell, J.; Froeba, M. Silica-Based Mesoporous Organic-Inorganic Hybrid Materials. *Angew. Chem. Int. Ed.* **2006**, 45, 3216-3251.
8. Farrell, R. A.; Petkov, N.; Morris, M.I A.; Holmes, J. D. Self-Assembled Templates for the Generation of Arrays of 1-Dimensional Nanostructures: From Molecules to Devices. *J. Colloid Interface Sci.* **2010**, 349, 449-472.
9. Di Renzo, F.; Galarneau, A.; Trens, P.; Fajula, F. In *Handbook of Porous Solids*; Schueth, F.; Sing, K. S. W.; Weitkamp, J., Eds.; Wiley-VCH, Weinheim, 2002, 3, pp 1311-1395.
10. Soler-Illia, G. J. d. A. A.; Crepaldi, E. L.; Grosso, D.; Sanchez, C. Block Copolymer-Templated Mesoporous Oxides. *Curr. Opin. Colloid Interface Sci.* **2003**, 8, 109-126.
11. Han, L.; Che, S. Anionic Surfactant Templated Mesoporous Silicas (AMSS). *Chem. Soc. Rev.* **2013**, 42, 3740-3752.

12. Wu, S.-H.; Mou, C.-Y.; Lin, H.-P. Synthesis of Mesoporous Silica Nanoparticles. *Chem. Soc. Rev.* **2013**, *42*, 3862-3875.
13. Kruk, M. Access to Ultralarge-Pore Ordered Mesoporous Materials through Selection of Surfactant/Swelling-Agent Micellar Templates. *Acc. Chem. Res.* **2012**, *45*, 1678-1687.
14. Stein, A.; Rudisill, S. G.; Petkovich, N. D. Perspective on the Influence of Interactions Between Hard and Soft Templates and Precursors on Morphology of Hierarchically Structured Porous Materials. *Chem. Mater.* **2014**, *26*, 259-276.
15. Kim, S.; Jacoby, J.; Stebe, M.-J.; Canilho, N.; Pasc, A. Solid Lipid Nanoparticle - Functional Template of Meso-Macrostructured Silica Materials. *ACS Symp. Ser.* **2015**, *1192*, 269-283.
16. Viau, L.; Neouze, M.-Al.; Biolley, C.; Volland, S.; Brevet, D.; Gaveau, P.; Dieudonne, P.; Galarneau, A.; Vioux, A. Ionic Liquid Mediated Sol-Gel Synthesis in the Presence of Water or Formic Acid: Which Synthesis for Which Material? *Chem. Mater.* **2012**, *24*, 3128-3134.
17. Li, L.-L.; Sun, L.-D.; Zhang, Y.-W.; Yan, C.-H. Functional-Template Directed Self-Assembly (FTDSA) of Mesostructured Organic-Inorganic Hybrid Materials. *Sci. China B* **2009**, *52*, 1759-1768.
18. Yao, B.; Zhao, D. Periodic Mesoporous Organosilicas. In *Encyclopedia of Inorganic and Bioinorganic Chemistry*; John Wiley & Sons Ltd.: Chichester, UK, 2011, pp 1-17.
19. Nukatsuka, I.; Kodate, K.; Iwasaki, K.; Aoki, H.; Kasahara, S.; Kitagawa, F. Spontaneous Formation of Mesoporous Silica Films Using Non-Surfactant Template, and Optimization with Doehlert Designs, for Adsorbent for Polycyclic Aromatic Hydrocarbons. *J. Sol-Gel Sci. Technol.* **2013**, *65*, 230-237.
20. Wang, Y.; Qi, W.; Wang, J.; Li, Q.; Yang, X.; Zhang, J.; Liu, X.; Huang, R.; Wang, M.; Su, R.; He, Z., Columnar Liquid Crystals Self-Assembled by Minimalistic Peptides for Chiral Sensing and Synthesis of Ordered Mesoporous Silica. *Chem. Mater.* **2018**, *30*, 7902-7911.

21. Wang, J.; Groen, J. C.; Coppens M.-O. Unified Formation Mechanism of Disordered Mesoporous Silica, Structured by Means of Nontemplating Organic Additives. *J. Phys. Chem. C* **2008**, 112, 19336-19345.
22. Ryzhakov, A.; Thi, T. D.; Stappaerts, J.; Bertoletti, L.; Kimpe, K.; Sa C., Andre R.; Saokham, P.; Van den Mooter, G.; Augustijns, P.; Somsen, G. W.; Kurkov, S.; Inghelbrecht, S.; Arien, A.; Jimidar, M.; Schrijnemakers, K.; Loftsson, T. Self-Assembly of Cyclodextrins and Their Complexes in Aqueous Solutions. *J. Pharm. Sci.* **2016**, 105, 2556-2569.
23. Polarz, S.; Smarsly, B.; Bronstein, L.; Antonietti, M. From Cyclodextrin Assemblies to Porous Materials by Silica Templating. *Angew. Chem. Int. Ed.* **2001**, 40, 4417-4421.
24. Bleta, R.; Ponchel, A.; Monflier, E. Cyclodextrin-Based Supramolecular Assemblies: a Versatile Toolbox for the Preparation of Functional Porous Materials. *Environ. Chem. Lett.* **2018**, 16, 1393-1413.
25. Saenger, W.; Jacob, J.; Gessler, K.; Steiner, T.; Hoffmann, D.; Sanbe, H.; Koizumi, K.; Smith, S. M.; Takaha, T. Structures of the Common Cyclodextrins and Their Larger Analogues – Beyond the Doughnut. *Chem. Rev.* **1998**, 98, 1787-1802.
26. *Spin Crossover in Transition Metal Compounds I–III* (Eds: P. Gülich, H. A. Goodwin), Springer, Berlin, Heidelberg **2004**.
27. M. A. Halcrow, *Spin-Crossover Materials: Properties and Applications*, John Wiley & Sons, Chichester, UK **2013**.
28. Kumar, K. S.; Ruben, M. Emerging Trends in Spin Crossover (SCO) Based Functional Materials and Devices. *Coord. Chem. Rev.* **2017**, 346, 176-205.
29. Molnar, G.; Rat, S.; Salmon, L.; Nicolazzi, W.; Bousseksou, A. Spin Crossover Nanomaterials: From Fundamental Concepts to Devices. *Adv. Mater.* **2018**, 30, 17003862.
30. Roubeau, O. Triazole-Based One-Dimensional Spin-Crossover Coordination Polymers. *Chem. Eur. J.* **2012**, 18, 15230-15244.

31. Grosjean, A.; Daro, N.; Kauffmann, B.; Kaiba, A.; Létard, J.-F.; Guionneau, P. The 1D Polymeric Structure of the $[\text{Fe}(\text{NH}_2\text{trz})_3](\text{NO}_3)_2 \cdot n\text{H}_2\text{O}$ (with $n=2$) Spin Crossover Compound Proven by Single Crystal Investigations. *Chem. Comm.* **2011**, 47, 12382-12384.
32. Bräunlich, I.; Sanchez-Ferrer, A.; Bauer, M.; Schepper, R.; Knüsel, P.; Dshemuchadse, J.; Mezzenga, R.; Caseri, W. Polynuclear Iron(II)-Aminotriazole Spincrossover Complexes (Polymers) In Solution. *Inorg. Chem.* **2014**, 53, 3546-3557.
33. Echeverria, C.; Rubio, M.; Mitchell, G. R.; Lopez, D. Structure of a Spin-Crossover Fe(II)-1,2,4-Triazole Polymer Complex Gel in Toluene. Small Angle Neutron Scattering and Viscoelastic Studies. *Eur. Polym. J.* **2014**, 53, 238-245.
34. Roubeau, O.; Colin, A.; Schmitt, V.; Clérac, R. Thermoreversible Gels as Magneto-Optical Switches. *Angew. Chem. Int. Ed.* **2004**, 43, 3283-3286.
35. Gaspar, A. B.; Seredyuk, M. Spin Crossover in Soft Matter. *Coord. Chem. Rev.* **2014**, 268, 41-58.
36. Matsukizono, H.; Kuroiwa, K.; Kimizuka, N. Lipid-Packaged Linear Iron(II) Triazole Complexes in Solution: Controlled Spin Conversion via Solvophobic Self-Assembly. *J. Am. Chem. Soc.* **2008**, 130, 5622-5623.
37. Kuroiwa, K.; Kimizuka, N. Self-Assembly and Functionalization of lipophilic Metal-Triazole Complexes in Various Media. *Polymer J.* **2013**, 45, 384-390.
38. Kume, S.; Kuroiwa, K.; Kimizuka, N. Photoresponsive molecular wires of Fe(II) Triazole Complexes in Organic Media and Light-Induced Morphological Transformations. *Chem. Comm.* **2006**, 2442-2444.
39. Voisin, H.; Aimé, C.; Vallée, A.; Bleuzen, A.; Schmutz, M.; Mosser, G.; Coradin, T.; Roux, C. Preserving the Spin Transition Properties of Iron-Triazole Coordination Polymers within Silica-Based Nanocomposites. *J. Mater. Chem. C* **2017**, 5, 11542-11550.

40. Zhao, T.; Cuignet, L.; Dirtu, M. M.; Wolff, M.; Spasojevic, V.; Boldog, I.; Rotaru, A.; Garcia, Y.; Janiak, C. Water Effect on the Spin-Transition Behavior of Fe(II) 1,2,4-Triazole 1D Chains Embedded in Pores of MCM-41. *J. Mater. Chem. C* **2015**, *3*, 7802-7812.
41. Faulmann, C.; Chahine, J.; Malfant, I.; De Caro, D.; Cormary, B.; Valade, L.; A Facile Route for the Preparation of Nanoparticles of the Spin-Crossover Complex [Fe(Htrz)₂(trz)](BF₄) in Xerogel Transparent Composite Film. *Dalton Trans.* **2011**, *40*, 2480-2485.
42. Durand, P.; Pillet, S.; Bendeif, E.-E.; Carteret, C.; Bouazaoui, M.; El Hamzaoui, H.; Capoen, B.; Salmon, L.; Hébert, S.; Ghanbaja, J.; Aranda, L.; Schaniel, D. Room Temperature Bistability with Wide Thermal Hysteresis in a Spin Crossover Silica Nanocomposite. *J. Mater. Chem. C* **2013**, *1*, 1933-1942.
43. Innocenzi, P.; Malfatti, L. Mesoporous Thin Films: Properties and Applications. *Chem. Soc. Rev.* **2013**, *42*, 4198-4216.
44. Cho, J.; Ishida, Y. Macroscopically Oriented Porous Materials with Periodic Ordered Structures: From Zeolites and Metal-Organic Frameworks to Liquid-Crystal-Templated Mesoporous Materials. *Adv. Mater.* **2017**, *29*, 1605974.
45. Grosso, D.; Cagnol, F.; Soler-Illia, G. J. d. A. A.; Crepaldi, E. L.; Amenitsch, H.; Brunet-Bruneau, A.; Bourgeois, A.; Sanchez, C. Fundamentals of Mesostructuring Through Evaporation-Induced Self-Assembly. *Adv. Funct. Mater.* **2004**, *14*, 309-322.
46. Walcarius, A.; Sibottier, E.; Etienne, M.; Ghanbaja, J. Electrochemically Assisted Self-Assembly of Mesoporous Silica Thin Films. *Nat. Mater.* **2007**, *6*, 602-608.
47. Teng, Z.; Zheng, G.; Dou, Y.; Li, W.; Mou, C.-Y.; Zhang, X.; Asiri, A. M.; Zhao, D. Highly Ordered Mesoporous Silica Films with Perpendicular Mesochannels by a Simple Stöber-Solution Growth Approach. *Angew. Chem. Int. Ed.* **2012**, *51*, 2173-2177.

48. Kao, K.-C.; Lin, C.-H.; Chen, T.-Y.; Liu, Y.-H.; Mou, C.-Y. A General Method for Growing Large Area Mesoporous Silica Thin Films on Flat Substrates with Perpendicular Nanochannels. *J. Am. Chem. Soc.* **2015**, *137*, 3779-3782.
49. Goux, A.; Etienne, M.; Aubert, E.; Lecomte, C.; Ghanbaja, J.; Walcarius, A. Oriented Mesoporous Silica Films Obtained by Electro-Assisted Self-Assembly. *Chem. Mater.* **2009**, *21*, 731-741.
50. Walcarius, A. Mesoporous Materials-Based Electrochemical Sensors. *Electroanalysis* **2015**, *27*, 1303-1340.
51. Yan, F.; Lin, X.; Su, B. Vertically Ordered Silica Mesochannel Films: Electrochemistry and Analytical Applications. *Analyst* **2016**, *141*, 3482-3495.
52. Zhou, Z.; Guo, W.; Xu, L.; Yang, Q.; Su, B. Two Orders-of-Magnitude Enhancement in the Electrochemiluminescence of Ru(bpy)₃²⁺ by Vertically Ordered Silica Mesochannels. *Anal. Chim. Acta* **2015**, *886*, 48-55.
53. Nasir, T.; Herzog, G.; Liu, L.; Hébrant, M.; Despas, C.; Walcarius, A. Mesoporous Silica Thin Films for Improved Electrochemical Detection of Paraquat. *ACS Sensors* **2018**, *3*, 484-493.
54. Li, C. L.; Iqbal, M.; Lin, J. J.; Luo, X. L.; Jiang, B.; Malgras, V.; Wu, K. C. W.; Kim, J.; Yamauchi, Y. Electrochemical Deposition: An Advanced Approach for Templated Synthesis of Nanoporous Metal Architectures. *Acc. Chem. Res.* **2018**, *51*, 1764-1773.
55. Li, C.; Jiang, B.; Miyamoto, N.; Kim, J. H.; Malgras, V.; Yamauchi, Y. Surfactant-Directed Synthesis of Mesoporous Pd Films with Perpendicular Mesochannels as Efficient Electrocatalysts. *J. Am. Chem. Soc.* **2015**, *137*, 11558-11561.
56. Wu, K. C. W.; Jiang, X.; Yamauchi, Y. New Trend on Mesoporous Films: Precise Controls of One-Dimensional (1D) Mesochannels Toward Innovative Applications. *J. Mater. Chem.* **2011**, *21*, 8934-8939.

57. Weng, W.; Higuchi, T.; Suzuki, M.; Fukuoka, T.; Shimomura, T.; Ono, M.; Radhakrishnan, L.; Wang, H.; Suzuki, N.; Oveisi, H.; Yamauchi, Y. A High-Speed Passive-Matrix Electrochromic Display Using a Mesoporous TiO₂ Electrode with Vertical Porosity. *Angew. Chem. Int. Ed.* **2010**, *49*, 3956-3959.
58. Oveisi, H.; Jiang, X.; Imura, M.; Nemoto, Y.; Sakamoto, Y.; Yamauchi, Y. A Mesoporous γ -Alumina Film with Vertical Mesoporosity: The Unusual Conversion from a 1m³m Mesostructure to Vertically Oriented γ -Alumina Nanowires. *Angew. Chem. Int. Ed.* **2011**, *50*, 7410-7413.
59. Vilà, N.; André, E.; Ciganda, R.; Ruiz, J.; Astruc, D.; Walcarius, A. Molecular Sieving with Vertically-Aligned Mesoporous Silica Films and Electronic Wiring Through Isolating Nanochannels. *Chem. Mater.* **2016**, *28*, 2511-2514.
60. Lin, X.; Yang, Q.; Yan, F.; Zhang, B.; Su, B. Gated Molecular Transport in Highly Ordered Heterogeneous Nanochannel Array Electrode. *ACS Appl. Mater. Interfaces* **2016**, *8*, 33343-33349.
61. Karman, C.; Vilà, N.; Walcarius, A. Amplified Charge Transfer for Anionic Redox Probes Through Oriented Mesoporous Silica Thin Films. *ChemElectroChem* **2016**, *3*, 2130-2137.
62. Serrano, M. B.; Despas, C.; Herzog, G.; Walcarius, A. Mesoporous Silica Thin Films for Molecular Sieving and Electrode Surface Protection Against Biofouling. *Electrochem. Commun.* **2015**, *52*, 34-36.
63. Yang, Q.; Lin, X.; Su, B. Molecular Filtration by Ultrathin and Highly Porous Silica Nanochannel Membranes: Permeability and Selectivity. *Anal. Chem.* **2016**, *88*, 10252-10258.
64. Zhou, L.; Hou, H.; Wei, H.; Yao, L.; Sun, L.; Yu, P.; Su, B.; Mao, L. In Vivo Monitoring of Oxygen in Rat Brain by Carbon Fiber Microelectrode Modified with Anti-fouling Nanoporous Membrane. *Anal. Chem.* **2019**, *91*, 3645-3651.
65. Etienne, M.; Goux, A.; Sibottier, E.; Walcarius, A. Oriented Mesoporous Organosilica Films on Electrode: a New Class of Nanomaterials for Sensing. *J. Nanosci. Nanotechnol.* **2009**, *9*, 2398-2406.

66. Vilà, N.; Ghanbaja, J.; Aubert, E.; Walcarius, A. Electrochemically Assisted Generation of Highly Ordered Azide-Functionalized Mesoporous Silica for Oriented Hybrid Films. *Angew. Chem. Int. Ed.* **2014**, *53*, 2945-2950.
67. Vilà, N.; Ghanbaja, J.; Walcarius, A. Clickable Bifunctional and Vertically-Aligned Mesoporous Silica Films. *Adv. Mater. Interfaces* **2016**, *3*, 1500440.
68. Nadzhafova, O.; Etienne, M.; Walcarius, A. Direct Electrochemistry of Hemoglobin and Glucose Oxidase in Electrodeposited Sol-Gel Silica Thin Films on Glassy Carbon. *Electrochem. Commun.* **2007**, *9*, 1189-1195.
69. Wang, Z.; Etienne, M.; Kohring, G.-W.; Bon Saint Côme, Y.; Kuhn, A.; Walcarius, A. Electrochemically Assisted Deposition of Sol-Gel Bio-Composite with Co-Immobilized Dehydrogenase and Diaphorase. *Electrochim. Acta* **2011**, *56*, 9032-9040.
70. Etienne, M.; Quach, A.; Grosso, D.; Nicole, L.; Sanchez, C.; Walcarius, A. Molecular Transport into Mesoporous Silica Thin Films: Electrochemical Monitoring and Comparison Between p6m, P6₃/mmc, Pm3n Structures. *Chem. Mater.* **2007**, *19*, 844-856.
71. Etienne, M.; Guillemin, Y.; Grosso, D.; Walcarius, A. Electrochemical Approaches for the Fabrication and/or the Characterization of Pure and Hybrid Templated Mesoporous Oxide Thin Films: A Review. *Anal. Bioanal. Chem.* **2013**, *405*, 1497-1512.
72. Ryabov, A. D.; Amon, A.; Gorbatova, R. K.; Ryabova, E. S.; Gnedenko, B. B. Mechanism of a "Jumping Off" Ferricenium in Glucose Oxidase-D-Glucose-Ferrocene Micellar Electrochemical Systems. *J. Phys. Chem.* **1995**, *99*, 14072-14077.
73. Guillemin, Y.; Etienne, M.; Aubert, E.; Walcarius, A. Electrogeneration of Highly Methylated Mesoporous Silica Thin Films With Vertically-Aligned Mesochannels and Electrochemical Monitoring of Mass Transport Issues. *J. Mater. Chem.* **2010**, *20*, 6799-6807.

74. Mazalov, L. N.; Asanov, I. P.; Varnek, V. A. Study of Electronic Structure of Spin-Transition Complexes by XPS and Mössbauer Spectroscopy. *J. Electron Spectrosc.* **1998**, *96*, 209-214.
75. Fettkenhauer, C.; Wang, X.; Kailasam, K.; Antonietti, M.; Dontsova, D. Synthesis of Efficient Photocatalysts for Water Oxidation and Dye Degradation Reactions Using CoCl_2 Eutectics. *J. Mater. Chem. A* **2015**, *3*, 21227-21232.
76. A Danyıldıza, Z.; Uzuna, D.; Calamb, T. T.; Hasdemir, E. Voltammetric Sensor Based on Glassy Carbon Electrode Modified With 1H-1,2,4-Triazole-3-thiol Coating for Rapid Determination of Trace Lead Ions in Acetate Buffer Solution. *J. Electroanal. Chem.* **2017**, *805*, 177-183.
77. Finšgar, M. EQCM and XPS Analysis of 1,2,4-Triazole and 3-Amino-1,2,4-Triazole as Copper Corrosion Inhibitors in Chloride Solution. *Corrosion Sci.* **2013**, *77*, 350-359.
78. He, R.; Wang, Z.; Tan, L.; Zhong, Y.; Li, W.; Xing, D.; Wei, C.; Tang, Y. Design and Fabrication of Highly Ordered Ion Imprinted SBA-15 and MCM-41 Mesoporous Organosilicas for Efficient Removal of Ni^{2+} From Different Properties of Wastewaters. *Microporous Mesoporous Mater.* **2018**, *257*, 212-221.
79. Furlani, A.; Russo, M. V.; Polzonetti, G.; Martin, K.; Wang, H. H.; Ferraro, J. R. Spectroscopic Studies of FeCl_3 -Doped Polymers of Polyphenylacetylene. *Appl. Spectrosc.* **1990**, *44*, 331-334.
80. Gupta, R. P.; Sen, S. K. Calculation of Multiplet Structure of Core p-Vacancy Levels. I. *Phys. Rev. B* **1974**, *10*, 71-77.
81. Gupta, R. P.; Sen, S. K. Calculation of Multiplet Structure of Core p-Vacancy Levels. II. *Phys. Rev. B* **1975**, *12*, 15-19.
82. Nesbitt, H. W.; Muir, I. J. X-ray Photoelectron Spectroscopic study of a Pristine Pyrite Surface Reacted With Water Vapour and Air. *Geochim. Cosmochim. Acta* **1994**, *58*, 4667-4679.
83. Jia, Q.; Han, H.; Wang, L.; Liu, B.; Yang, H.; Shen, J. Effects of CTAC Micelles on the Molecular Structures and Separation Performance of Thin-Film Composite (TFC) Membranes in Forward Osmosis Processes. *Desalination* **2014**, *340*, 30-41.

84. Nasir, T.; Zhang, L.; Vilà, N.; Herzog, G.; Walcarius, A. Electrografting of 3-Aminopropyltriethoxysilane on Glassy Carbon Electrode for the Improved Adhesion of Vertically Oriented Mesoporous Silica Thin Films. *Langmuir* **2016**, *32*, 4323-4332.
85. Nakamoto, A.; Kojima, N.; Jun, L. X.; Moritomo, Y.; Nakamura, A. Demonstration of the Thermally Induced High Spin–Low Spin Transition for a Transparent Spin Crossover Complex Film [Fe(II)(H-trz)₃]-Nafion (trz = triazole). *Polyhedron* **2005**, *24*, 2909-2912.
86. Etienne, M.; Goubert-Renaudin, S.; Rousselin, Y.; Marichal, C.; Denat, F.; Lebeau, B.; Walcarius, A. Multiarm Cyclam-Grafted Mesoporous Silica: A Strategy to Improve the Chemical Stability of Silica Materials Functionalized With Amine Ligands. *Langmuir* **2009**, *25*, 3137-3145.
87. Trivedi, M. K.; Tallapragada, R. M.; Branton, A.; Trivedi, D.; Nayak, G.; Mishra, R. K.; Jana, S. Characterization of Physical, Spectral and Thermal Properties of Biofield Treated 1,2,4-Triazole. *J. Mol. Pharm. Org. Process Res.* **2015**, *3*, 128.
88. Mokadem, Z.; Mekki, S.; Saïdi-Besbes, S.; Agusti, G.; Elaissari, A.; Derdour, A. Triazole Containing Magnetic Core-Silica Shell Nanoparticles for Pb²⁺, Cu²⁺ and Zn²⁺ Removal. *Arabian J. Chem.* **2017**, *10*, 1039-1051.
89. Shacham, R.; Avnir, D.; Mandler, D. Electrodeposition of Methylated Sol-Gel Films on Conducting Surfaces. *Adv. Mater.* **1999**, *11*, 384-388.
90. Sibottier, E.; Sayen, S.; Gaboriaud, F.; Walcarius, A. Factors Affecting the Preparation and Properties of Electrodeposited Silica Thin Films Functionalized With Amine or Thiol Groups. *Langmuir* **2006**, *22*, 8366-8373.
91. Kamebuchi, H.; Jo, T.; Shimizu, H.; Okazawa, A.; Enomoto, M.; Kojima, N. Development of pH-Sensitive Spin-crossover Iron(II) Complex Films, [Fe(II)(diAMsar)]–Nafion: Manipulation of the Spin State by Proton Concentration. *Chem. Lett.* **2011**, *40*, 888889.

92. Wang, Z.; Etienne, M.; Quilès, F.; Kohring, G.-W.; Walcarius, A. Durable Cofactor Immobilization in Sol-Gel Bio-Composite Thin Film for Reagentless Biosensors Using Dehydrogenases. *Biosensors Bioelectron.* **2012**, *32*, 111-117.
93. Fattakhova Rohlfig, D.; Rathousky, J.; Rohlfig, Y.; Bartels, O.; Wark, M. Functionalized Mesoporous Silica Films as a Matrix for Anchoring Electrochemically Active Guests. *Langmuir* **2005**, *21*, 11320-11329.
94. Font, J.; de March, P.; Busque, F.; Casas, E.; Benitez, M.; Teruel, L.; Garcia, H. Periodic Mesoporous Silica Having Covalently Attached Tris(Bipyridine)Ruthenium Complex: Synthesis, Photovoltaic and Electrochemiluminescent Properties. *J. Mater. Chem.* **2007**, *17*, 2336-2343.
95. Rafiee, M.; Karimi, B.; Farrokhzadeh, S.; Vali, H. Hydroquinone Functionalized Oriented MCM-41 Mesochannels at the Electrode Surface. *Electrochim. Acta* **2013**, *94*, 198-205.
96. Song, C.; Villemure, G. Electrode Modification With Spin-Coated Films of Mesoporous Molecular Sieve Silicas. *Microporous Mesoporous Mater.* **2001**, *44-45*, 679-689.
97. Edler, K. J.; Reynolds, P. A.; Branton, P. J.; Trouw, F.; White, J. W. The Structure and Dynamics of Hydrogen Adsorption in Mesoporous MCM-41. *J. Chem. Soc. Faraday Trans.* **1997**, *93*, 1667-1674.